Proceedings of the VI National Conference of Neutron Scattering, Chlewiska, Poland, June 14–18, 2009

Molecular Reorientations of *N*-*n*-Hexyltetrachlorophthalimide Studied by ^{1}H NMR

K. Hołderna-Natkaniec*, K. Jurga, A. Woźniak-Braszak and A. Walczak

Department of Physics, Adam Mickiewicz University, Umultowska 85, 61-614 Poznań, Poland

The spin–lattice relaxation times T_1 and the second moment of ^{1}H NMR line have been employed to study the internal dynamics of protons of *N*-*n*-hexyltetrachlorophthalimides in the temperature range 80–350 K. The model of internal reorientations has been proposed.

PACS numbers: 07.05.Tp, 31.15.E−, 33.20.Ea, 64.70.K−, 76.60.−k

1. Introduction

N-*n*-hexyltetrachlorophthalimide, of the chemical formula $(C_8Cl_4NO_2)(C_6H_{13})$ belongs to biologically active compounds as phthaloyl derivatives. The structure activity relationship studies of *N*-*n*-alkyltetrachlorophthalimides have shown that the hydrophobic groups at nitrogen atom are of crucial importance for their activity. It has recently been shown that tetrachlorophthalimide ($C_8Cl_4NO_2$) derivatives are good glucosidase inhibitors [1–4]. The subject of our studies was the internal dynamics of hexyl derivative of tetrachlorophthalimide. The aim of this study was to find the relationship between the phase transition and internal dynamics of the hexyl chain (C_6H_{13}), i.e. the determination of the activation energies of internal reorientation of terminal methyl group and the hexyl group and estimated their barrier heights of internal reorientation by quantum chemistry (QC) methods.

The spin–lattice relaxation times, T_1, and second moment of the ^{1}H NMR line, M_2, were employed to study proton dynamics of *N*-*n*-hexyltetrachlorophthalimides in the temperature range 90–350 K.

2. Methods

The differential scanning calorimetry (DSC) measurements were carried out using a Perkin-Elmer DSC 7 instrument. About 4.8 mg of $C_{14}H_{13}Cl_4NO_2$ was packed into a stainless steel DSC cell. The heating and the cooling rate was 10 K/min. The DSC measurements performed in the temperature range 98–303 K indicated a phase transition at 156 K/170 K on cooling/heating, respectively. Figure 1 shows the DSC diagram in the vicinity of the phase transition temperature.

To analyze molecular dynamics with ^{1}H NMR method it is necessary to know the location of protons. The structural study performed by the X-ray diffraction (XRD) method [1] produces results with a big margin of error, because of low density of electron clouds of hydrogen, therefore calculations of the molecule structure by quantum chemistry methods had been done. The structure of an isolated molecule was optimised by different methods, starting from the atom–atom 6–12 potential [5], to semi-empirical PM3 [6], and finally to density functional theory (DFT) method with hybrid functional B3LYP and 6-311G** basis set [7] and then the internal frequencies of normal vibrations were calculated. Both the calculated structures of the molecule skeleton were compared with the one determined by the XRD method, as well as the IR vibrational frequencies and intensities of normal modes calculated by DFT method were compared with the experimental ones, to check quality of the optimised structure. The IR spectra was taken in KBr using the Bruker spectrometer. The QC optimisation of the structure, as well as the calculation of the vibrational spectra, were performed using Gaussian'03 package [8] by the Supercomputer and Network Centre PCSS in Poznań.

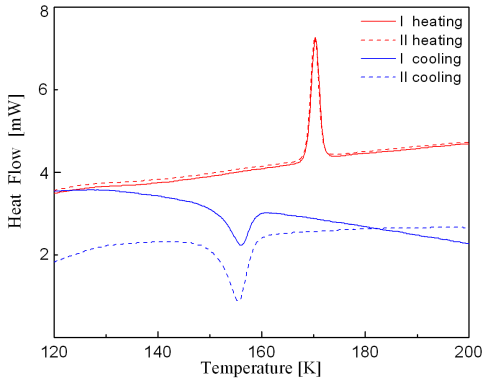

Fig. 1. The DSC diagram of *N*-*n*-hexyltetrachlorophthalimide.

The spin–lattice ^{1}H NMR relaxation time T_1 in the laboratory frame measurements were carried out on a home-made pulse spectrometer operating at 30.2 MHz [9],

* corresponding author; e-mail: natkanie@amu.edu.pl

using the saturation method with the pulse sequence $n\times\pi/2$–τ–$\pi/2$. The studied sample was degassed for several hours in the glass ampoule and sealed under vacuum. The absorption signal from the rf field was measured in the range of 90–350 K on a laboratory made instrument [10] operating in the double modulation system.

3. Results and discussion

3.1. Optimisation of the structure

Figure 2 presents the structure of the isolated molecule together with the atoms numbering. In order to analyze the experimental data, the structure of the isolated molecule was optimised by the DFT method with B3LYP/6-311G** basis set, as well as by semi-empirical PM3 method using the Gaussian 03 software. Table I collects the optimized bond lengths and angles together with the X-ray crystal structure data [1]. The structure of a skeleton of isolated molecule was also compared with that of *N*-*n*-butyltetrachlorophtalamide determined by XRD at the room temperature [2]. The building of tetrachlorophthalimide moiety of both compounds is close. The quality of the structural parameters agreement with the experimental ones may be expressed by the root mean square deviation σ of the predicted parameters defined as:

$$\sigma = \sum \left(\left((X_{\text{predicted}} - X_{\text{exp}})^2 \Big/ N \right)^{1/2} \right), \qquad (1)$$

where X can be either bond lengths, bond angles or frequencies of normal modes (in angstrom, degree, or cm^{-1}, respectively) and N is the number of analyzed parameters. The hydrogen position was determined by the XRD method with significant error because of their low density of electron clouds. Consequently, the structure of carbon skeleton (without hydrogens) was used for comparison. As follows from Table I, the σ obtain the values: 0.021 Å, 1.3° and 0.027 Å, 2.3° for DFT and PM3 methods, respectively. The best reliable bond lengths values are given by the DFT/B3LYP/6-311G** calculations. The observed agreement between optimised structures of an isolated molecule (after DFT/B3LYP/6-311G** method) with the X-ray data means weak intermolecular interactions.

TABLE I

The comparison of the bond lengths and the internal angles of isolated molecule of $(C_8Cl_4NO_2)(C_6H_{13})$ given by X-ray data [1] and optimised by different quantum chemistry methods.

	Bond length determined at room temperature by X-ray diffraction study of $(C_8Cl_4NO_2)(C_4H_9)$ [2]	Bond length determined at room temperature by X-ray diffraction study of $(C_8Cl_4NO_2)(C_6H_{13})$ [1]	Bond length optimized by DFT methods B3LYP/ 6-311G** in isolated molecule approximation of $(C_8Cl_4NO_2)(C_6H_{13})$	Bond length optimized by PM3 methods in isolated molecule approximation of $(C_8Cl_4NO_2)(C_6H_{13})$
Bond length in [Å]				
N1–C2	1.398	1.392	1.395	1.453
N1–C10	1.466	1.462	1.461	1.476
C7–C8	1.381	1.380	1.384	1.381
C8–C9	1.501	1.497	1.503	1.493
C2–O	1.205	1.202	1.204	1.201
C–Cl		1.723, 1.719, 1.714, 1.721	1.731, 1.733, 1.733, 1.731	1.689, 1.699, 1.699, 1.689
C–C in heptyl chain		1.503, 1.458, 1.543 1.500, 1.515, 1.462	1.530, 1.523, 1.532 1.531, 1.531, 1.461	1.540, 1.512. 1.520 1.521, 1.512, 1.476
Bond angles				
C9–N1–C10		122.5	123.5	123.3
N1–C10–C11		112.0	112.8	110.2
N1–C2–C3	123.6	112.0	115.4	116.3
C3–C4–C5		118.3	118.9	118.2
C5–C6–C7		118.1	120.9	120.8
C6–C7–C8		120.1	120.5	118.0
C9–C8–C7	111.6	130.7	130.4	130.3
O–C9–N1	125.2	125.3	125.3	124.1
C–C–C in hexyl chain		112.5, 111.7, 112.6, 113.1, 112.8	112.8. 112.2, 113.0, 113.5, 113.1	111, 111.4, 111.3, 111, 113
H–C–H on hexyl chain		107.8, 107.8, 107.6, 107.6, 107.5, 107.6, 109.5, 109.5, 109.5	108.5, 106.9, 106.0, 105.9, 105.9, 107.5, 107.5, 107.5, 107.8	109.8, 108.0, 108.0, 109.9, 111.7, 111.7, 107.6, 107.6, 107.6

TABLE II

Normal modes of *N*-*n*-hexyltetrachlorophthalimide observed in IR spectra at room temperature and calculated by DFT and PM3 methods.

Frequencies of normal modes in [cm^{-1}]				Proposed assignment and PED [%]	
Experimental	Calculated				
IR	B3LYP/6-311G**	IR intensity	PM3		
	13.6	0.0			
	20.4	0.05			
	33.6	0.01	56.1	χ [C5–C4], χ [C7–C6]	36
				χ [C4–C3], χ [C8–C7]	37
	58.9	0.02	61.5	χ [C11–C12]	31
	62.4	0.04	70.8	χ [C10–C11]	31
	67.5	0.02	80.0	χ [N1–C10]	50
	85.7	0.01	85.3	χ [N1–C10]	33
	93.5	1.33	91.6	χ [C3–C2], χ [C8–C9]	24
				χ [C2–N1], χ [N1–C9]	28
	120.2	0.02	121.3	χ [C12–C13]	53
	130.7	2.21	128.4	χ [C13–C14]	29
	138.4	0.01	135.6	υ [C11–C12]	26
	151.4	2.41	142.6	χ [C2–N1], χ [N1–C9]	9
				ρ [C4–C5–Cl], ρ [C5–C6–C7]	16
				ρ [C5–C4–C3], ρ [C8–C7–C6]	20
				ρ [C4–C3–C8], ρ [C3–C8–C7]	33
	167.0	0.02	147.7	δ [Cl–C5–C6], δ [C5–C4–Cl]	10
				δ [C3–C4–Cl]	8
				δ [C4–C3–C2], δ [C7–C8–C9]	18
	198.3	0.40	177.2	δ [C4–C5–Cl], δ [C7–C6–Cl]	29
				δ [Cl–C5–C6], δ [C5–C4–Cl]	54
				δ [C3–C4–Cl]	11
	219.0	0.06	181.1	δ [C4–C5–Cl], δ [C7–C6–Cl]	33
				δ [Cl–C5–C6], δ [C5–C4–Cl]	36
				δ [C3–C4–Cl]	12
	233.8	2.40	182.7	δ [Cl–C5–C6], δ [C5–C4–Cl]	38
				δ [C3–C4–Cl]	26
	235.7	0.07	244.8	χ [C14–C15]	90
	244.9	0.01	248.0		
	271.9	0.48	285.4	δ [N1–C2–O], δ [N1–C9–O]	9
				δ [C2–N1–C10], δ [C9–N1–C10]	42
	288.7	1.55	289.0	ρ [C4–C5–Cl], ρ [C5–C6–C7]	17
	299.3	1.35	292.0	υ [C4–Cl], υ [C7–Cl]	8
				δ [C5–C4–C3], δ [C8–C7–C6]	11
	321.7	3.63	312.2	υ [C5–Cl], υ [C6–Cl]	43
				δ [C4–C5–C6], δ [C5–C6–C7]	20
	328.7	0.02	321.3	ρ [C4–C5–Cl], ρ [C5–C6–C7]	17
				ρ [C4–C3–C8], ρ [C3–C8–C7]	13
	348.4	0.02	333.0	υ [C4–Cl], υ [C7–Cl]	45
				δ [N1–C2–O], δ [N1–C9–O]	13
	349.2	0.00	333.9	ρ [C5–C4–C3], ρ [C8–C7–C6]	48
				ρ [C4–C3–C8], ρ [C3–C8–C7]	16
	378.6	0.26	359.2	υ [C5–Cl], υ [C6–Cl]	12
				υ [C4–Cl], υ [C7–Cl]	34
				δ [C3–C2–O], δ [C8–C9–O]	11

TABLE II cont.

Frequencies of normal modes in [cm^{-1}]				Proposed assignment and PED [%]	
Experimental	Calculated				
IR	B3LYP/6-311G**	IR intensity	PM3		
408.8	407.7	25.83	413.7	υ [C5–Cl]	20
				υ [C2–C3]	7
470.5	441.3	3.6	469.4	δ [C15–C14–H], δ [C13–C14–H],	6
				δ [C12–C13–H]	
490.8	515.0	18.15	496.0	υ [C5–Cl], υ [C6–Cl]	23
				δ [N1–C2–O13], δ [N1–C9–O10]	7
	542.8	0.01	520.0	ρ [C4–C5–Cl], ρ [C5–C6–C7]	25
				ρ [C4–C3–C8], ρ [C3–C8–C7]	18
				ρ [C3–C2–N1], ρ [C8–C9–N1]	42
512.0	597.9	3.24	577.8	υ [C4–Cl12], υ [C7–Cl11]	29
				δ [C4–C5–Cl15], δ [C7–C6–Cl14]	12
				δ [Cl15–C5–C6], δ [C5–C4–Cl12]	
				δ [C6–C7–Cl11], δ [C5–C6–Cl14]	24
587.2	624.9	1.12	588.4	δ [C3–C2–N1], δ [C8–C9–N1]	17
626.8	632.0	12.82	606.3	ρ [C4–C5–Cl], ρ [C5–C6–C7]	16
				ρ [C5–C4–C3], ρ [C8–C7–C6]	47
				ρ [C3–C2–N1], ρ [C8–C9–N1]	18
686.6	685.5	0.01	688.4	υ [C5–Cl15], υ [C6–Cl]	26
				υ [C4–Cl12], υ [C7–Cl]	30
				δ [C8–C3–C2], δ [C3–C8–C9]	10
700.0	700.1	6.5	695.8	δ [C8–C3–C2], δ [C3–C8–C9]	17
				δ [C3–C2–O], δ [C8–C9–O]	14
				δ [N1–C2–O], δ [N1–C9–O]	10
734.8	732.1	99.7	703.4	υ [C5–Cl], υ [C6–Cl]	41
				υ [C4–Cl], υ [C7–Cl]	14
	734.1	23.8	719.9	ρ [C4–C5–Cl], ρ [C5–C6–C7]	54
				ρ [C5–C4–C3], ρ [C8–C7–C6]	12
				ρ [C3–C2–N1], ρ [C8–C9–N1]	24
753.1	739.7	0.7	729.4	ρ [C5–C4–C3], ρ [C8–C7–C6]	13
				ρ [C4–C3–C8], ρ [C3–C8–C7]	16
				ρ [C3–C2–N1], ρ [C8–C9–N1]	57
767.8	772.6	16.4	743.8	δ [C15–C14–H], δ [C13–C14–H],	39
				δ [C12–C13–H]	
				δ [C14–C13–H], δ [C14–C13–H]	10
	773.2	1.17	773.8	δ [C15–C14–H], δ [C15–C14–H]	11
				δ [C15–C14–H], δ [C13–C14–H],	24
				δ [C12–C13–H]	
802.2	781.1	0.68	821.8	δ [C15–C14–H], δ [C15–C14–H]	16
814.8				δ [C15–C14–H], δ [C13–C14–H],	26
				δ [C12–C13–H]	
				δ [C14–C15–H], δ [C14–C15–H],	14
				δ [C14–C15–H]	
	811.4	11.6	854.6	ρ [C4–C5–Cl], ρ [C5–C6–C7]	21
				ρ [C5–C4–C3], ρ [C8–C7–C6]	46
				ρ [C4–C3–C8], ρ [C3–C8–C7]	20

TABLE II cont.

Frequencies of normal modes in [cm^{-1}]				Proposed assignment and PED [%]	
Experimental	Calculated				
IR	B3LYP/6-311G**	IR intensity	PM3		
881.3	883.5	7.09	875.5	υ [C4–Cl], υ [C7–Cl]	29
				υ [C2–N1], υ [N1–C9]	8
				δ [C5–C4–C3], δ [C8–C7–C6]	15
	894.1	3.18	891.1	δ [C15–C14–H], δ [C13–C14–H],	
				δ [C12–C13–H]	19
				δ [C14–C15–H]	13
				δ [C14–C13–H]	9
905.4, 945.0	901.5	0.28	924.7	υ [C5–Cl], υ [C6–Cl]	18
996.1	950.0	0.08	941.8	δ [C14–C15–H], δ [C14–C15–H],	64
				δ [C14–C15–H]	
999.9	1002.3	8.6	962.3	δ [C15–C14–H], δ [C13–C14–H2],	47
				δ [C12–C13–H]	
1019.2	1012.3	10.2	986.5		
1033.7	1037.3	7.45	1046.6	υ [C3–C2], υ [C8–C9]	10
				δ [N1–C10–H], δ [N1–C10–H]	16
1048.1	1045.0	4.32	1064.6	δ [C15–C14–H], δ [C13–C14–H],	
				δ [C12–C13–H]	
1076.1	1057.4	3.86	1087.9	δ [C15–C14–H], δ [C15–C14–H]	19
				δ [C15–C14–H], δ [C13–C14–H]	38
				δ [C14–C15–H], δ [C14–C15–H]	11
				δ [C10–C11–H], δ [C10–C11–H]	16
	1067.3	0.39	1089.2	δ [C15–C14–H], δ [C13–C14–H]	10
				δ [C11–C10–H]	10
	1094.7	52.4	1103.8	δ [C15–C14–H]	25
				δ [C15–C14–H], δ [C13–C14–H]	13
				δ [C12–C13–H]	10
				δ [C14–C15–H]	20
				δ [C11–C10–H]	20
				δ [C10–C11–H]	
1120.5	1142.0	9.2	1105.2	δ [C15–C14–H], δ [C13–C14–H],	42
1163.9				δ [C12–C13–H]	
1172.5				δ [C14–C15–H], δ [C14–C15–H],	13
1182.2				δ [C14–C15–H]	
				δ [C14–C13–H], δ [C14–C13–H]	24
1199.5	1163.6	16.22	1112.8	δ [C15–C14–H], δ [C13–C14–H],	12
				δ [C12–C13–H]	
1223.7	1200.5	161.00	1125.9	δ [C15–C14–H]	11
				δ [C15–C14–H], δ [C13–C14–H],	19
				δ [C12–C13–H]	
1244.9	1217.5	6.23	1132.7	δ [C15–C14–H], δ [C13–C14–H]	9
				δ [C12–C13–H]	
				δ [C14–C15–H], δ [C14–C15–H],	10
				δ [C14–C15–H]	
1278.6	1265.6	6.57	1133.7	δ [C15–C14–H] δ [C13–C14–H]	55
				δ [C12–C13–H]	
				δ [C14–C13–H], δ [C14–C13–H]	11
				δ [C10–C11–H], δ [C10–C11–H]	12

TABLE II cont.

Frequencies of normal modes in [cm^{-1}]				Proposed assignment and PED [%]	
Experimental	Calculated				
IR	B3LYP/6-311G**	IR intensity	PM3		
	1271.0	1.57	1136.2	δ [C15–C14–H], δ [C13–C14–H], δ[C12–C13–H]	46
				δ [C14–C13–H], δ [C14–C13–H]	14
				δ [C14–C13–H], δ [C14–C13–H]	28
1298.9	1318.1	68.21	1161.4	υ [C2–N1], υ [N1–C9]	43
				δ [N1–C10–H], δ [N1–C10–H]	20
	1319.5	0.50	1171.5	δ [C15–C14–H], δ [C13–C14–H], δ [C12–C13–H]	29
				δ [C14–C13–H], δ [C14–C13–H]	11
				δ [C14–C13–H], δ [C14–C13–H]	11
				δ [N1–C10–H], δ [N1–C10–H]	11
	1335.6	3.45	1209.7	δ [C15–C14–H], δ [C13–C14–H], δ[C12–C13–H]	27
				δ [C14–C13–H], δ [C14–C13–H]	16
				δ [N1–C10–H], δ [N1–C10–H]	14
1335.5	1347.7	1.52	1221.6	υ [C3–C2], υ [C8–C9]	29
				υ [C2–N1], υ [N1–C9]	17
				δ [C5–C4–C3], δ [C8–C7–C6]	11
				δ [C4–C3–C8], δ [C3–C8–C7]	11
	1353.0	0.00	1264.4	δ [C15–C14–H], δ [C13–C14–H], δ [C12–C13–H]	24
1358.7	1371.6	148.24	1293.6	υ [C5–C4], υ [C7–C6], δ [C15–C14–H], δ [C13–C14–H]	10
				δ [C12–C13–H]	12
1372.2	1376.2	141.859	1311.2	δ [C11–C10–H]	11
	1386.3	154.9	1331.3	δ [C15–C14–H], δ [C13–C14–H], δ[C12–C13–H]	19
				δ [H–C14–H], δ [H–C13–H], δ [H31–C12–H]	29
				δ [C14–C15–H]	11
				δ [H–C15–H]	12
1388.5	1392.1	61.223	1338.6	δ [C15–C14–H], δ [C13–C14–H], δ [C12–C13–H]	10
				δ [H–C13–H], δ [H–C12–H]	66
1406.9	1396.7	227.18	1352.9	δ [H–C14–H], δ [H–C13–H] δ [H–C12–H]	50
				δ [C10–C11–H]	10
	1413.8	2.74	1360.3	δ [H–C15–H], υ [H–C15–H]	95
	1426.6	7.98	1362.3	δ [H–C15–H]	89
1436.8	1428.6	46.88	1368.2	δ [C15–C14–H], δ [C13–C14–H], δ [C12–C13–H]	11
				δ [H–C14–H], δ [H–C13–H], δ [H–C12–H]	59
1450	1486.4	31.61	1378.3	δ [C15–C14–H], δ [C13–C14–H], δ [C12–C13–H]	8
				δ [H–C14–H], δ [H–C13–H], δ [H–C12–H]	56

TABLE II cont.

Frequencies of normal modes in [cm^{-1}]				Proposed assignment and PED [%]	
Experimental	Calculated				
IR	B3LYP/6-311G**	IR intensity	PM3		
	1499.8	0.56	1390.4	δ [H–C14–H], δ [H–C13–H],	15
				δ [H–C12–H]	
				δ [C14–C15–H], δ [C14–C15–H],	10
				δ [C14–C15–H]	
				δ [H–C15–H], δ [H–C15–H],	10
				δ [H–C15–H]	
	1500.7	0.61	1401.4	υ [C2–N1], υ [N1–C9]	6
				δ [C15–C14–H], δ [C13–C14–H]	6
				δ [C12–C13–H]	
				δ [H–C15–H], δ [H–C15–H],	5
				δ [H–C15–H]	
	1509.9	1.16	1419.3	δ [C15–C14–H], δ [C13–C14–H],	18
				δ[C12–C13–H]	
				δ [C14–C13–H], δ [C14–C13–H]	6
1520	1518.4	8.83	1441.4	υ [C5–Cl], υ [C6–Cl]	10
				υ [C4–C3], υ [C8–C7]	17
	1520.3	2.20	1523.9	υ [C5–C4], υ [C7–C6]	60
	1528.3	11.54	1546.0	υ [C5–C4], υ [C7–C6]	12
				υ [C4–C3], υ [C8–C7]	32
				υ [C3–C2], υ [C8–C9]	21
	1590.9	0.07	1771.1	υ [C5–C4], υ [C7–C6]	10
				υ [C4–C3], υ [C8–C7]	27
1583.2	1593.3	7.90	1791.0	υ [C5–C4] υ [C7–C6]	17
				υ [C4–C3] υ [C8–C7]	59
1636.4	1789.2	512.01	1957.4	υ [C2–O], υ [C9–O]	89
1744.3	1838.7	84.13	2012.5	υ [C3–C2], υ [C8–C9]	6
				υ [C2–O], υ [C9–O]	87
	3001.9	0.01	2835.3	υ [C13–H], υ [C12–H]	18
				υ [C10–H]	65
				υ [C11–H]	16
	3005.3	3.96	2841.0	υ [C14–H]	12
				υ [C13–H], υ [C12–H]	65
				υ [C10–H]	21
	3015.6	67.13	2850.1	υ [C14–H]	34
				υ [C13–H], υ [C12–H]	40
				υ [C10–H]	10
				υ [C11–H]	17
	3019.6	0.21	2857.3	υ [C14–H]	32
				υ [C13–H], υ [C12–H]]	17
				υ [C11–H]	46
	3025.3	43.51	2859.8	υ [C14–H]	20
				υ [C13–H], υ [C12–H]	59
				υ [C11–H]	20
	3031.6	0.18	2887.5	υ [C10–H]	99
2792.9	3032.2	40.43	2918.3	υ [C13–H], υ [C12–H]	82
				υ [C11–H]	15

TABLE II cont.

Frequencies of normal modes in [cm^{-1}]				Proposed assignment and PED [%]	
Experimental	Calculated				
IR	B3LYP/6-311G**	IR intensity	PM3		
	3051.5	31.55	2922.2	υ[C13–H], υ[C12–H]	32
				υ[C11–H]	62
2851.4	3072.3	34.20	2922.5	υ[C13–H], υ[C12–H]	77
				υ[C11–H]	22
	3076.2	29.83	2926.2	υ[C14–H]	98
2870.7	3085.6	88.55	2973.0	υ[C15–H]	99
2924.7	3089.5	54.31	2979.5	υ[C15–H]	99
2953.6	3126.5	9.73	3065.1	υ[C15–H]	99
3468					

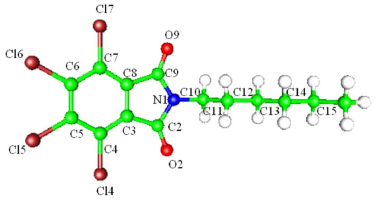

Fig. 2. The atom notation of isolated molecule of *N*-*n*-hexyltetrachlorophthalimide.

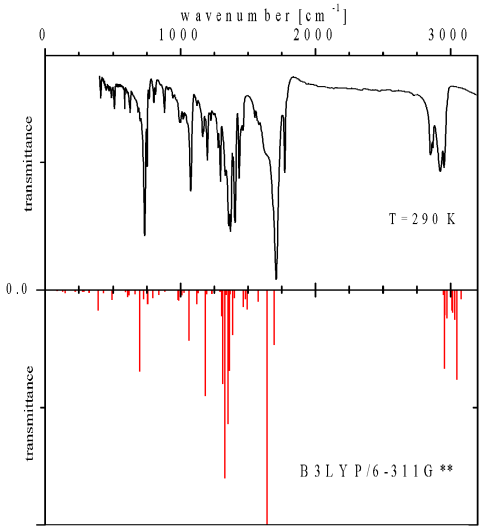

Fig. 3. The IR spectra of *N*-*n*-hexyltetrachlorophthalimide recorded at room temperature and calculated by B3LYP/6-311G** method, without scaling.

In order to verify the optimised structure of the studied molecular system, the middle infrared (IR) spectra were recorded at room temperature and compared with the calculated ones by the quantum chemistry methods. The root mean square deviation σ of the predicted frequencies and experimental ones according to Eq. (1) was 70 and 95 cm^{-1} for DFT and PM3 methods, respectively. The experimental IR spectrum was in agreement with the results presented by Brycki et al. [1]. Figure 3 shows the experimental and calculated by DFT/B3LYP/6-311G** spectra.

Table II collects the harmonic vibrational modes computed by different QC methods and corresponding experimental values. The intensities of calculated bands were also given. The proposed assignments of the normal vibrations modes were collected together with the value of potential energy distribution (PED) in %. The torsional out-of-plane modes χ were predicted below 130 cm^{-1}. They were unobserved in our IR experimental spectra. The torsional out-of-plane vibrations of the methyl group χ[C(14)–C(15)H$_3$] should be at 235 cm^{-1}.

The deformational in-plane δ and out-of-plane ρ vibrational modes assigned to tetrachlorophthalimide moiety were predicted at 441 and (739, 773 cm^{-1}), while in experimental IR spectrum they appeared at 470 and (753, 767 cm^{-1}), respectively. The deformational in plane modes of δ[C–C–C] of the hexyl group were calculated in the range 773–1271 cm^{-1}.

The strongest bands assigned as stretching υ[C=O] was predicted by DFT calculation at 1789 and 1838 cm^{-1} (without scaling) and they were observed at 1636 and 1775 cm^{-1}. Figure 4 gives the comparison of calculated frequencies and intensities of IR active normal modes with the experimental IR data. The slope of this dependence is 0.95, which means small effect of anharmonicity.

In order to propose the model of internal motion, the calculations of energy of isolated moiety *versus* the methyl group reorientation (a), the ethyl chain-end of the hexyl group (b) and alkyl chain reorientation (c) were performed by semi-empirical PM3 method as less time

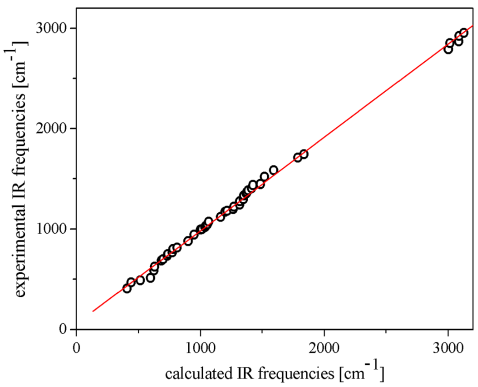

Fig. 4. Comparison of calculated by DFT/B3LYP/6-311G** method frequencies of IR active normal modes and experimental room temperature IR spectra of *N-n-*-hexyltetrachlorophthalimide.

consuming. These results were presented in Fig. 5. The barrier height of the threefold methyl group reorientation is estimated as 6.5 kJ/mol (Fig. 5a). The inequivalent minima of the energy for *trans–gauche* isomerization of ethyl chain-end group, denoted as E_{A} and E_{B}, for $E = 22.4$ kJ/mol and $\Delta E = 4.2$ kJ/mol were given (Fig. 5b). These calculations, performed in the isolated molecule approximation, give the suggestion on different energy barrier for methyl group reorientation, *trans–gauche* isomerization and fourfold reorientation.

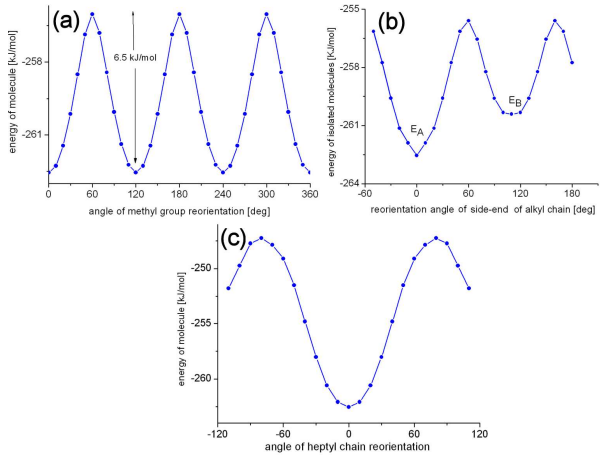

Fig. 5. The energy of the isolated molecule, calculated by the semi-empirical PM3 method vs. the methyl-group reorientation (a), the *trans–gauche* reorientation of the hexyl chain (b), and alkyl-chain reorientation (c).

3.2. Proton second moment

The line width and the second moment of ^{1}H NMR line are parameters usually used to characterize the absorption signal in rf field. The second moment of the experimental signal was calculated according to the formula

$$M_2 = \frac{\int_0^\infty (H - H_0)^2 f(H)\,\mathrm{d}H}{\int_0^\infty f(H)\,\mathrm{d}H}\,. \qquad (2)$$

Figure 6 shows the temperature dependence of the second moment M_2 and the slope line width of ^{1}H NMR line for the compound studied. The signal was averaged and corrected for the second modulation amplitude. The measurements were made at first on heating the sample from 90 up to 350 K, and later on cooling. Temperature hysteresis of the second moment and the slope line width of the ^{1}H NMR line close to the phase transition temperature were observed. The value of the second moment changed from $(22.6 \pm 1.5) \times 10^{-8}$ T^2 at 90 K to $(4.4 \pm 0.5) \times 10^{-8}$ T^2 at 350 K. At the phase transition temperature the second moment changed jump-like from $(18.5 \pm 1.5) \times 10^{-8}$ T^2 to $(15.5 \pm 1.5) \times 10^{-8}$ T^2.

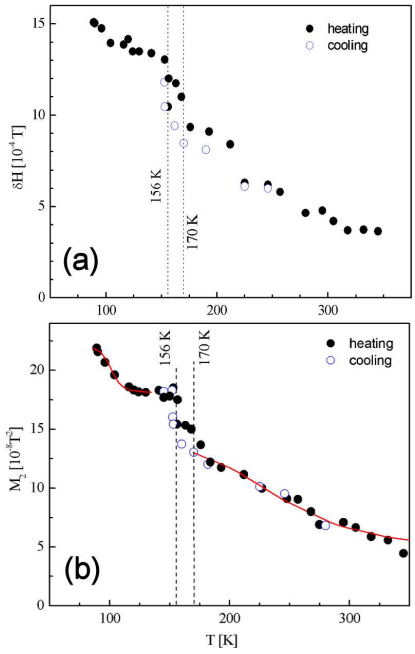

Fig. 6. The temperature dependence of the slope line width δH (a) and the second moment M_2 (b) of ^{1}H NMR line for *N-n*-hexyltetrachlorophthalimide.

In order to propose the model of internal dynamics, the spin–lattice relaxation time and the second moment of the ^{1}H NMR line were calculated in terms of the dipole–dipole Bloembergen–Purcell–Pound (BPP) theory [11]. The second moment of the ^{1}H NMR line was calculated taking into account the structure of the isolated molecule optimised by DFT/B3LYP/6-311G** method using Gaussian'03 package [8] (Table I).

The equation for the dipolar second moment M_2 was given by van Vleck [12] as

$$M_2^{\mathrm{rig}} = \frac{3}{5}\gamma_I^2\hbar^2 I\,(I+1)\,\frac{1}{N}\sum_{j,k}^{N}\frac{1}{r_{jk}^6}$$

$$+\frac{4}{15}\gamma_S^2\hbar^2 S\left(S+1\right)\frac{1}{N}\sum_{\mathrm{I,S}}^{\mathrm{N}}\frac{1}{r_{\mathrm{IS}}^6}\,, \tag{3}$$

where γ_I and γ_S are the gyromagnetic coefficient of the resonant spin I and the nonresonant spin S, respectively. The first contribution describes the interaction between homonuclear spins, while the second — interaction between the heteronuclear spins. The identification of the motional process responsible for narrowing of the ^{1}H NMR lines is performed by comparing the experimental values of M_2 with those calculated according to the van Vleck formula of dipolar theory for different models of internal motions. The sum of intra- and inter-molecular contributions $M_2 = M_2^{\mathrm{intra}} + M_2^{\mathrm{inter}}$ were compared with the experimental data. The intermolecular part of the M_2^{inter} was estimated according to the formula $M_2^{\mathrm{inter}} = 358.081 \times 4\pi dN_0/(3R^3m)$ [13], where density d is 1.5334 g/cm^3, m is mass of the molecule $= 612\times10^{-24}$ g, the cut-off radius R is 4 Å as the inter-chain distance. Consequently, M_2^{inter} is close to 0.65×10^{-8} T^2.

The onset of the molecular group reorientation around distinguished axis with a frequency of an order of the line width of the ^{1}H NMR line is the reason of the reduction of the second moment value from low temperature value for the "rigid lattice" M_2^{rig} to M_2^{reo} by a coefficient Δ_1:

$$\Delta_1 = \frac{M_2^{\mathrm{reo}}}{M_2^{\mathrm{rig}}} = \left(\frac{1-3\cos^2\beta_{jk}}{2}\right)^2, \tag{4}$$

where β_{jk} is the angle between the inter-proton vector in the molecular group undergoing reorientation and the axis of rotation [14]. When proton jumps between two inequivalent positions, the reduction coefficient Δ_2 is

$$\Delta_2 = 1 - \frac{3a}{(1+a)^2}\,,$$

where the parameter $a = \exp\left(\frac{E_{\mathrm{B}}-E_{\mathrm{A}}}{RT}\right)$ depends on the depth of the nearest potential barrier E_{A} and E_{B}.

After *trans–gauche* reorientation the value of the M_2 decreased, according to the formula [15, 16]:

$$M_2 = M_2^{\mathrm{rig}} - \frac{a}{(1+a)^2}\Delta M_{2,2}^0 \times\left[-1+\frac{2}{\pi}\arctan\left(\gamma_I\tau_{\mathrm{c}2}\sqrt{M_2}\right)\right], \tag{5}$$

where a depends on the depth of the nearest potential barrier E_{A} and E_{B}, and $\tau_{\mathrm{c}2}$ is the correlation time over the jump between the two unequal positions, $\Delta M_{2,2}$ is the change in the second moment value for *trans–gauche* isomerization.

The calculations of the second moment of the ^{1}H NMR line were performed taking into account the homonuclear interactions; the heteronuclear interactions were negligible in the discussion, as they give only 0.02×10^{-8} T^2. The intramolecular homonuclear contribution to the second moment of ^{1}H NMR line calculated for the rigid structure was 21.1×10^{-8} T^2 and the intermolecular contribution was estimated as 0.8×10^{-8} T^2. The total value of the second moment of ^{1}H NMR line was estimated to be 21.9×10^{-8} T^2, close to that observed $(22.6\pm1.5)\times10^{-8}$ T^2 at 90 K for the title compound. The second moment changes were interpreted assuming the following model of internal dynamics:

— reorientations of the terminal methyl group around the C_3 axis,

— the *trans–gauche* isomerization of the ethyl chain-end group,

— the reorientation of the whole alkyl chain.

The observed plateau of 18.5×10^{-8} T^2 is in good agreement with the calculated 15.7×10^{-8} T^2 value for the rigid chain with methyl group undergoing threefold reorientation. In the vicinity of phase transition temperature the *trans–gauche* isomerization of ethyl chain-end gives the reduction of the second moment of 2.7×10^{-8} T^2 in Eq. (5) when the $\Delta E = 8$ kJ/mol and $E = 16$ kJ/mol. This mechanism finds confirmation in the crystal structure data [1]. One may find the short contact between carbons C(11) and C(13) (Fig. 2) from hexyl chain and oxygen O(2) from tetrachlorophthalimide moiety of the length 3.397 and 3.553 Å, respectively. Above the phase transition temperature, the second moment starts to decrease on heating. This indicates the appearance of the new motional mechanism. The onset of rotation of the whole alkyl chain about the C4 axis with a frequency of an order of a few kHz takes place. Then, the value of $M_2^{\mathrm{C4}} = (4.4\pm0.5)\times10^{-8}$ T^2 taken at 350 K can be related to the axial reorientation of the whole chain with the frequency higher than ^{1}H NMR line width taken at 350 K.

Taking into regard the above estimated values of the second moment plateau corresponding to the reorientations of the hexyl group, it is possible to determine the activation energies of these processes by fitting the Gutowsky and Pake [17] dependence $\tau_{\mathrm{c}} = \frac{2\pi}{\gamma_H\sqrt{M_2}}\tan\left(\frac{\pi}{2}\frac{M_2-B^2}{C^2-B^2}\right)$ (describing the temperature dependence of the correlation time found from the line shape changes expressed by the second moment of ^{1}H NMR line changes, when C^2 and B^2 are the value of second moment before and after thermal narrowing, respectively) to the experimental data with the lowest value of χ^2. In Fig. 6b the solid line represents the results of such fit below the phase transition temperature. The analysis of $M_2(T)$ gives the barrier height for the methyl group reorientations about the C3 axis as 13 kJ/mol.

A decrease in M_2 from 14×10^{-8} T^2 to 4×10^{-8} T^2 in temperature range (170 K, 290 K) can be related to the onset of chain reorientations about the C4 axis and the activation energy of this process is close to 32 kJ/mol.

3.3. Spin–lattice relaxation time

Figure 7 presents the temperature dependence of the spin–lattice relaxation time for the studied compound. The magnetisation recovery was single-exponential in the whole range of temperatures, to the accuracy of 3%. The T_1 curve shows the minimum of 67 ms at 133 K, which is slightly asymmetrical with a smaller slope on the low-temperature side. The minimum value of T_1 was calcu-

lated as 65 ms, according to Eq. (6) for $\omega\tau_c \approx 0.616$, taking into account the inter-proton distance in the methyl group as 1.79 Å, and it was assigned to the chain-end methyl group reorientation about the C3 axis.

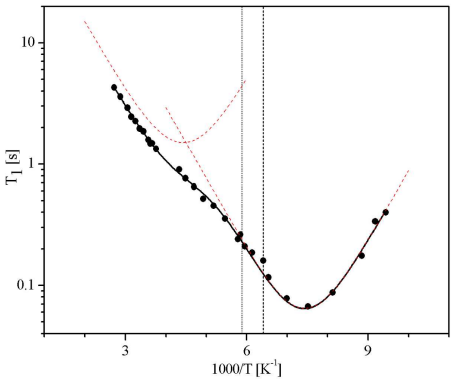

Fig. 7. The temperature dependence of the spin–lattice relaxation time T_1 for *N-n*-hexyltetrachlorophthalimide.

When we consider the reorientation of an isolated methyl group, the spin–lattice relaxation rate is

$$\left(\frac{1}{T_1}\right)^{\mathrm{CH_3}} = \frac{2}{3}\gamma_I^2 \Delta M_{2,1} \times \left(\frac{\tau_{c,1}}{1+\omega_0^2\tau_{c,1}^2} + \frac{4\tau_{c,1}}{1+4\omega_0^2\tau_{c,1}^2}\right), \quad (6)$$

where $\Delta M_{2,1} = M_2^{\mathrm{rigid}} - M_2^{\mathrm{motion}} = 4.5 \times 10^{-8}$ T^2 is the change in the second moment value accompanying the onset of the methyl group rotation of hexyl chain-end of the studied molecule, τ_{c1} is the correlation time of methyl group reorientation. This model satisfactorily describes experimental data in the low temperature phase.

In order to explain the experimental results above 150 K the *trans–gauche* reorientation of the chain-ends ethyl were taken into account. The potential wells calculated for these motions were shown in Fig. 5b. This relaxation rate of *trans–gauche* isomerization was described by the contribution [11, 12]:

$$\left(\frac{1}{T_1}\right)^{\text{trans–gauche}} = \frac{2}{3}\gamma_I^2 \Delta M_{2,2} \frac{4a}{(1+a)^2} \times \left(\frac{\tau_{c2}}{1+\omega_0^2\tau_{c2}^2} + \frac{4\tau_{c2}}{1+4\omega_0^2\tau_{c2}^2}\right). \quad (7)$$

The best fit judged as that with the lowest χ^2 of Eqs. (6) and (7) to the experimental relaxation times in the whole temperature range is presented as a continuous line in Fig. 7, while the partial contributions are presented as dotted lines. We estimated the activation energy for CH_3 reorientation as 10 kJ/mol, the correlation time $\tau_{01} = 3 \times 10^{-13}$ s and $\Delta M_{21} = 4.4 \times 10^{-8}$ T^2, while for the *trans–gauche* isomerization of the chain as $E_{a2} = 19$ kJ/mol, $\Delta E = 9$ kJ/mol, $\tau_{02} = 2 \times 10^{-13}$ s and $\Delta M_{22} = 2 \times 10^{-8}$ T^2. Table III collects the motional parameters thus obtained. The sequence of onset of internal reorientations were in qualitative agreement with predicted ones from the calculations performed in isolated molecule approximation.

TABLE III

Motional parameters from the temperature studies of of *N-n*-hexyltetrachlorophthalimide determined by ^{1}H NMR methods.

Motion	$M_2^{\mathrm{intra}} + M_2^{\mathrm{inter}}$ calc. [$\times 10^{-8}$ T^2]		M_2^{exp} [$\times 10^{-8}$ T^2]	Motional parameters			
					M_2	T_1	Simul.
rigid	21.1	0.8	22.6 ± 1.5				
C3 of CH_3	15.7	0.6	18.5 ± 1.5	E_{a1} [kJ/mol] τ_{01} [s]	13 ± 2	10 ± 2 3×10^{-13}	6.5
CH_2CH_3	13.2	0.5					
trans-gauche	13.0	0.6	15.5 ± 1.5	E_{a2} [kJ/mol] Δ [kJ/mol] τ_{02} [s]	16 ± 3 8 ± 2	19 ± 3 9 ± 2 2×10^{-13}	6 2.5
C4	5	0.2	5 ± 0.5	E_{a3} [kJ/mol]	32 ± 5		15

4. Summary

The phase transition was recorded at 156 K/170 K on cooling/heating, respectively. On heating the following reorientations were subsequently set on: the end-side chain methyl group, the *trans–gauche* isomerization of ethyl chain-end, and the rotation of the whole alkyl chain. ^{1}H NMR studies revealed the dynamics involved in dif-

ferent phases and gave the activation parameters of the subsequent motions taking place with the frequencies of the subsequent line widths.

Acknowledgments

The QC calculations were performed at PSCC in Poznań.

References

[1] B. Brycki, I. Kowalczyk, A. Zielinski, T. Borowiak, I. Wolska, *J. Mol. Struct.* **874**, 145 (2008).

[2] T. Borowiak, I. Wolska, B. Brycki, A. Zieliński, I. Kowalczyk, *J. Mol. Struct.* **833**, 197 (2007).

[3] S. Sou, S. Mayumi, H. Takahashi, R. Yamasaki, S. Kadoya, M. Sodeoka, Y. Hashimoto, *Bioorg. Med. Chem. Lett.* **10**, 1081 (2000).

[4] H. Takahashi, S. Sou, R. Yamasaki, M. Sodeoka, Y. Hashimoto, *Chem. Pharm. Bull.* **48**, 1494 (2000).

[5] A.I. Kitajgorodsky, *Molecular Crystal and Molecules*, Academic Press, New York 1973.

[6] J.J.P. Stewart, *J. Mol. Model.* **10**, 155 (2004); J.J.P. Stewart, *J. Comp. Chem.* **12**, 320 (1991); J.J.P. Stewart, *J. Comp. Chem.* **10**, 209 (1989); J.J.P. Stewart, *J. Comp. Chem.* **10**, 221 (1989).

[7] A.D. Becke, *J. Chem. Phys.* **97**, 9173 (1992); A.D. Becke, *J. Chem. Phys.* **98**, 5648 (1993); C. Lee, W. Yang, R.G. Parr, *Phys. Rev. B* **37**, 785 (1988).

[8] Gaussian 03, Revision D.01, M.J. Frisch, G.W. Trucks, H.B. Schlegel, G.E. Scuseria, M.A. Robb, J.R. Cheeseman, J.A. Montgomery, Jr., T. Vreven, K.N. Kudin, J.C. Burant, J.M. Millam, S.S. Iyengar, J. Tomasi, V. Barone, B. Mennucci, M. Cossi, G. Scalmani, N. Rega, G.A. Petersson, H. Nakatsuji, M. Hada, M. Ehara, K. Toyota, R. Fukuda, J. Hasegawa, M. Ishida, T. Nakajima, Y. Honda, O. Kitao, H. Nakai, M. Klene, X. Li, J.E. Knox, H.P. Hratchian, J.B. Cross, V. Bakken, C. Adamo, J. Jaramillo, R. Gomperts, R.E. Stratmann, O. Yazyev, A.J. Austin, R. Cammi, C. Pomelli, J.W. Ochterski, P.Y. Ayala, K. Morokuma, G.A. Voth, P. Salvador, J.J. Dannenberg, V.G. Zakrzewski, S. Dapprich, A.D. Daniels, M.C. Strain, O. Farkas, D.K. Malick, A.D. Rabuck, K. Raghavachari, J.B. Foresman, J.V. Ortiz, Q. Cui, A.G. Baboul, S. Clifford, J. Cioslowski, B.B. Stefanov, G. Liu, A. Liashenko, P. Piskorz, I. Komaromi, R.L. Martin, D.J. Fox, T. Keith, M.A. Al-Laham, C.Y. Peng, A. Nanayakkara, M. Challacombe, P.M.W. Gill, B. Johnson, W. Chen, M.W. Wong, C. Gonzalez, J.A. Pople, Gaussian Inc., Wallingford CT, 2004.

[9] K. Jurga, *J. Phys. E, Sci. Instrum.* **14**, 555 (1981).

[10] K. Hołderna-Matuszkiewicz, W. Wanarski, J. Klimowski, *Acta Phys. Pol. A* **59**, 477 (1981).

[11] N. Bloembergen, E.M. Purcell, R.V. Pound, *Phys. Rev.* **73**, 679 (1948).

[12] J.H. Van Vleck, *Phys. Rev.* **74**, 1168 (1948).

[13] G.W. Smith, *J. Chem. Phys.* **42**, 4229 (1965).

[14] G.W. Slichter, *Principles of Magnetic Resonance*, Springer-Verlag, Heidelberg 1978.

[15] E.R. Andrew, L. Latanowicz, *J. Magn. Reson.* **68**, 232 (1986); E.C. Reynhardt, *Chem. Phys. Lett.* **256**, 548 (1996).

[16] L. Latanowicz, E.C. Reynhardt, *J. Magn. Reson. Series A* **121**, 23 (1996).

[17] H.S. Gutowsky, G.E. Pake, *J. Chem. Phys.* **18**, 162 (1950).